

Statistical Efficiency of Target Localization from Angle and Shockwave Measurements

RICHARD W. OSBORNE, III
YAAKOV BAR-SHALOM
JEMIN GEORGE
LANCE KAPLAN

This work derives the Cramer-Rao lower bound (CRLB) for an acoustic target and sensor localization system in which the noise characteristics may depend on the location of the source. The system itself has been previously examined, but without deriving the CRLB and showing the statistical efficiency of the estimator used. Three different versions of the CRLB are derived, one in which direction of arrival (DOA) and (shockwave based) range measurements are available (“local estimate” based CRLB), one in which two types of DOA measurements and the time difference between them is available (“native measurement” based CRLB), and one in which only DOA measurements (bearing) are available (“bearings-only” CRLB). In each case, the estimator is found to be statistically efficient; but, depending on the sensor-target geometry, the range measurements may or may not significantly contribute to the accuracy of target localization. Additionally, the native measurements are found to result in superior localization when compared to the use of the range estimates.

Manuscript received May 30, 2013; revised January 14, 2014; released for publication October 14, 2014.

Refereeing of this contribution was handled by Ramona Georgescu.

This work was supported by the Army Research Office under contract W911NF-06-1-0467.

There are no conflict-of-interest or financial disclosure statements to be made at this time.

Authors' addresses: R. Osborne and Y. Bar-Shalom, Department of Electrical and Computer Engineering, University of Connecticut, 371 Fairfield Way, U-2157, Storrs, CT 06269 (e-mail: {rosborne, ybs}@enr.uconn.edu); J. George and L. Kaplan, Sensors and Electron Devices Directorate, U.S. Army Research Laboratory, 2800 Powder Mill Rd., Adelphi, MD 20783, (e-mail: {jemin.george, lance.m.kaplan}@us.army.mil)

1557-6418/14/\$17.00 © 2014 JAIF

1. INTRODUCTION

In any estimation system the ultimate goal is to extract the maximum information from the available data. The Fisher information matrix (FIM) provides a measure of the total information available from the observations of the system, and its inverse provides the Cramer-Rao lower bound (CRLB) [2]. A statistically efficient estimator is one in which the (co)variance of the estimation error meets the CRLB, and, therefore, extracts all of the available information from the observations.

The CRLB and statistical efficiency of an acoustic localization system will be examined here, based on the system described in [9], [10], which is meant to estimate the location of the source of a detected gunshot. Each sensor node of the system is assumed to provide an estimated bearing (direction of arrival—DOA) to the target, and, if the sensor node lies within a certain field of view (FOV) around the path of the bullet, a range estimate and bullet trajectory estimate as well. The range and bullet trajectory estimates are provided via a nonlinear transformation of the “native” measurements consisting of the bearing, a shockwave DOA measurement, and a time difference of arrival (TDOA) between the two DOA measurements. For those sensors that provide estimated range, the noise variance will be highly dependent on the position of the source. Each sensor node's local estimates (or, alternatively, its native measurements) are passed to a fusion center to perform the overall estimation of the target position. The sensor locations can also be simultaneously estimated with the target (source) location, but the improvement is negligible. It is also possible to remove the sensor locations from the estimation performed at the fusion center, but the inaccuracy of the sensor locations must then be explicitly accounted for in the CRLB derivations.

A number of papers have examined the problem of target localization in passive sensor environments, including [3], [7], [8], [18], [22], [24], [25]. The work of [24] generalizes the results of [7] to include sensor position uncertainty; however, neither paper examines the CRLB to see whether the estimator is statistically efficient. In [3], [8], [18], [25], different applications of localization with passive sensors are studied that also consider the CRLB. However, in [25], no estimation scheme is shown to meet the CRLB. In [8] the maximum likelihood (ML) estimation scheme examined is shown to be statistically efficient only when a significant number of measurements are used. In none of the above-mentioned papers were cases of position-dependent measurement noise considered.

Specific research pertaining to the acoustic localization of small-arms fire is examined in [1], [5], [9]–[17], [20], [21], [23]. In most of these works, CRLB/efficiency analysis is not performed. References

[11], [23] use the “local estimates,” while the remainder use either “native measurements” or only time-of-arrival (TOA) or TDOA measurements. Additionally, [13], [14], [16], [17] employ a bullet deceleration model. The work of [1] examined the effect of assuming an (incorrect) constant velocity bullet model and demonstrated modest localization errors for realistic scenarios. Of the previously mentioned work, only [5], [12], [16] perform any analysis of the CRLB. In [12], the CRLB is examined, but only in the case of native measurements. Reference [5] examines a method of localization using only TDOA measurements and derives the CRLB; however, the CRLB is shown to provide only a loose bound, with inaccurate cross-range performance prediction. Reference [16] also used TDOA measurements without DOA and derived the CRLB, but did not present results statistically demonstrating efficiency, though it was mentioned that simulations indicated their estimator met the bound for TDOA accuracy below a given threshold.

In this work, the CRLB of the central estimator (fuser) is derived for three cases: a “bearings-only” case, which assumes that only bearing measurements are available from the sensor nodes; a “local estimate” case, which assumes that range and bullet trajectory estimates are available in addition to bearing; and a “native measurement” case, which assumes that the two previously mentioned types of DOA measurements (to the shooter and the shockwave) and the TDOA are available.

Section 2 provides an overview of the system in question, and examines the probability distribution and density of the range estimate errors from the individual sensors. Section 3 provides the expressions necessary to evaluate the CRLB for the problem in question, both with and without the position-dependent noise terms. Section 4 describes the simulation scenarios and provides the results. Finally, Section 5 concludes the paper.

2. LOCALIZATION SYSTEM OVERVIEW

The system to be examined here is the same as the one described in [9], [10] except that we also consider the use of native measurements. A brief overview of the system is provided here, however, to introduce the concepts and notations.

A number of acoustic sensors are placed throughout a surveillance region with the intent of detecting gunfire and estimating the position of the source. The target (source) location will be denoted as

$$T = [T_x \quad T_y]' \quad (1)$$

and the i th sensor location is denoted as

$$S_i = [S_{ix} \quad S_{iy}]' \quad (2)$$

The problem is assumed constrained to a two-dimensional plane for simplicity.

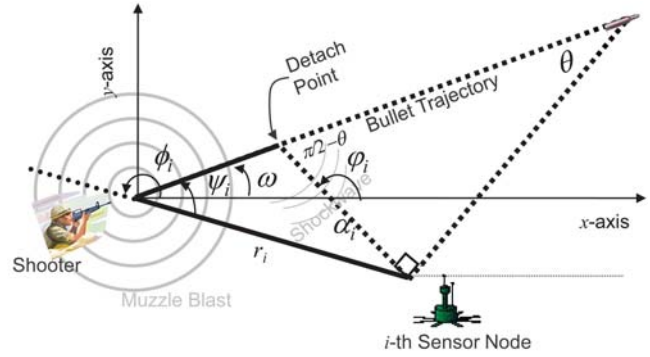


Fig. 1. Geometry of the bullet trajectory and the DOA angles of the muzzle blast and shockwave as seen by the i th sensor node.

2.1. Sensor Nodes

Each sensor will be assumed to provide at most five *native measurements*

$$\zeta_i = [\hat{\phi}_i \quad \hat{\phi}_s \quad \hat{\tau}_i]' \quad (3)$$

and

$$\hat{S}_i = [\hat{S}_{ix} \quad \hat{S}_{iy}]' \quad (4)$$

where $\hat{\phi}_i$ is the DOA angle to the shooter, based on the detection of the muzzle blast; $\hat{\phi}_s$ is the DOA angle of the shockwave from the bullet; $\hat{\tau}_i$ is the TDOA between the muzzle blast and the shockwave; and \hat{S}_i is the noisy sensor location (obtained via a GPS sensor at each node).¹ The DOA measurements are assumed to be measured counter-clockwise (CCW) from the x -axis of a global reference coordinate system, to which each sensor is assumed to be aligned. Each measurement is assumed to be corrupted by zero-mean Gaussian noise, with standard deviations of σ_ϕ , σ_ϕ , σ_τ , σ_{ix} and σ_{iy} , respectively. The overall geometry of the various angular measurements involved are depicted in Figure 1.

The shockwave (and therefore the TDOA measurement) is only visible to sensor nodes that are within a limited FOV around the path of the bullet, depicted in Figure 2. The FOV is $\pi - 2\theta$ [6], where

$$\theta = \sin^{-1} \left(\frac{1}{m} \right) \quad (5)$$

and m is the Mach number of the bullet, assumed here to be $m = 2$ [12]. Note that in this work, a constant velocity bullet model is considered.

The target bearing from the i th sensor node is

$$\phi_i = \tan^{-1} \left(\frac{T_y - S_{iy}}{T_x - S_{ix}} \right) \quad (6)$$

and the DOA angle of the shockwave is

$$\varphi_i = \begin{cases} -\frac{\pi}{2} - \theta + \omega & \text{if } \pi + \omega < \phi_i < \frac{3\pi}{2} - \theta + \omega \\ \frac{\pi}{2} + \theta + \omega & \text{if } \frac{\pi}{2} + \theta + \omega < \phi_i < \pi + \omega \end{cases} \quad (7)$$

¹We use similar notation and terminology as in [9], [10].

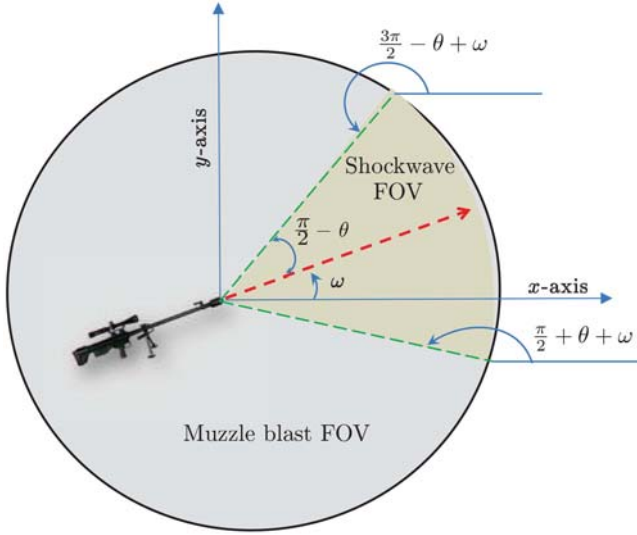


Fig. 2. Field of view (FOV) of the muzzle blast and shockwave DOA angles.

where ω is the angle of the trajectory (counter-clockwise) with respect to the x -axis.

Using the *native measurements*, the sensors can compute the *local estimates*²

$$z_i = [\hat{\phi}_i \quad \hat{r}_i \quad \hat{\omega}_i]' \quad (8)$$

where [9], [10]

$$\hat{r}_i = \frac{c\hat{\tau}_i}{1 - \cos(\hat{\phi}_i - \hat{\varphi}_i)} \quad (9)$$

is the estimated target range, c is the speed of sound (assumed to be known perfectly), and $\hat{\omega}_i$ is the estimated bullet trajectory angle. In view of (7), the estimated bullet trajectory can be obtained directly from $\hat{\varphi}_i$ and the standard deviation of $\hat{\omega}_i$ is σ_φ .

Sensor i sends its measured location (4), and either the native measurements (3) or the local estimates (8) to a fusion center, to estimate the source location T .

The variance of the range estimate (which is location dependent) can be approximated as (similar to [9], [10])

$$\sigma_{r_i}^2(T, \hat{S}_i, \omega) \approx \nabla r_i \begin{bmatrix} \sigma_\tau^2 & 0 \\ 0 & \sigma_\phi^2 + \sigma_\varphi^2 \end{bmatrix} \nabla r_i' \quad (10)$$

where

$$\nabla r_i = \begin{bmatrix} \frac{\partial r_i}{\partial \tau} & \frac{\partial r_i}{\partial(\phi - \varphi)} \end{bmatrix} \quad (11)$$

and

$$\frac{\partial r_i}{\partial \tau} = \frac{c}{1 - \cos(\phi_i - \varphi_i)} \quad (12)$$

$$\frac{\partial r_i}{\partial(\phi - \varphi)} = -\frac{r_i \sin(\phi_i - \varphi_i)}{1 - \cos(\phi_i - \varphi_i)} \quad (13)$$

²The angular measurements of (8) are also assumed to be measured CCW from the x -axis of the global reference frame.

The likelihood function of T , S_i , and ω given the estimate z_i is

$$\Lambda_{z_i}(T, S_i, \omega) \triangleq p(z_i | T, S_i, \omega) \approx \mathcal{N}(z_i; \mu_{z_i}, \Sigma_{z_i}) \quad (14)$$

where

$$\mu_{z_i} = [\phi_i \quad r_i \quad \omega]' \quad (15)$$

and, since the noise on ω is the same as the noise on φ in view of (7), and is the same for all i ,

$$\Sigma_{z_i}(T, \hat{S}_i, \omega) = \begin{bmatrix} \sigma_\phi^2 & \text{cov}(r_i, \phi_i) & 0 \\ \text{cov}(r_i, \phi_i) & \sigma_{r_i}^2(T, \hat{S}_i, \omega) & \text{cov}(r_i, \omega) \\ 0 & \text{cov}(r_i, \omega) & \sigma_\varphi^2 \end{bmatrix} \quad (16)$$

with (see Appendix A)

$$\text{cov}(r_i, \phi_i) = -\frac{r_i \sin(\phi_i - \varphi_i)}{1 - \cos(\phi_i - \varphi_i)} \sigma_{\phi_i}^2 \quad (17)$$

$$\text{cov}(r_i, \omega_i) = \frac{r_i \sin(\phi_i - \varphi_i)}{1 - \cos(\phi_i - \varphi_i)} \sigma_{\varphi_i}^2 \quad (18)$$

The errors in (14) are assumed to be uncorrelated across the sensors.

The likelihood function of T , S_i , and ω given the native measurements ζ_i is

$$\Lambda_{\zeta_i}(T, S_i, \omega) \triangleq p(\zeta_i | T, S_i, \omega) = \mathcal{N}(\zeta_i; \mu_{\zeta_i}, \Sigma_{\zeta_i}) \quad (19)$$

where

$$\mu_{\zeta_i} = [\phi_i \quad \varphi_i \quad \tau_i]' \quad (20)$$

and

$$\Sigma_{\zeta_i} = \begin{bmatrix} \sigma_\phi^2 & 0 & 0 \\ 0 & \sigma_\varphi^2 & 0 \\ 0 & 0 & \sigma_\tau^2 \end{bmatrix} \quad (21)$$

The likelihood function of S_i is

$$\Lambda_{S_i}(S_i) \triangleq p(\hat{S}_i | S_i) = \mathcal{N}(\hat{S}_i; S_i, \Sigma_{S_i}) \quad (22)$$

where

$$\Sigma_{S_i} = \begin{bmatrix} \sigma_{ix}^2 & 0 \\ 0 & \sigma_{iy}^2 \end{bmatrix} \quad (23)$$

The sensors are assumed to obtain their locations, albeit imperfectly, from GPS.³ Additionally, the sensors are assumed to be aligned to a common reference frame (e.g., via compass readings, where any error/bias present is assumed to be identical across sensors due to the small area involved). For the sensors, the GPS localization serves as a prior and guarantees complete observability for the target-sensor complex. The final estimates of the sensor locations can be only slightly improved over their initial GPS estimates, but the improvement this makes to the final target localization is

³If the sensor position estimates contain a common (slowly varying) bias across sensors (a reasonable assumption since these sensors are not too far from each other), the relative sensor registration will be unaffected and the target estimate will exhibit the same bias.

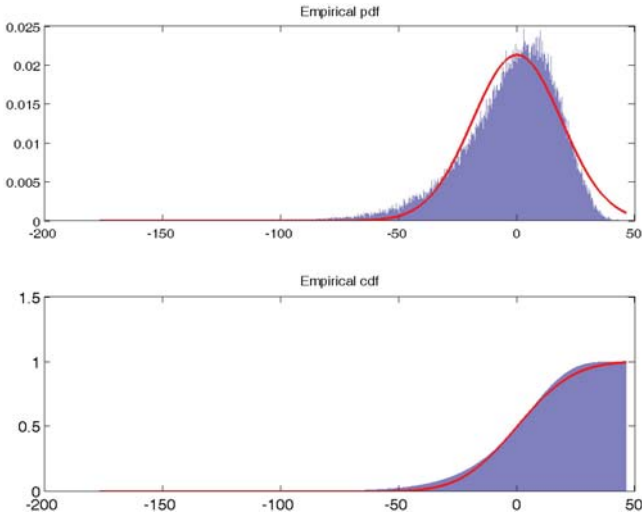


Fig. 3. Empirical pdf and cdf of \tilde{r}_i for Sensor 1 of Scenario 3.

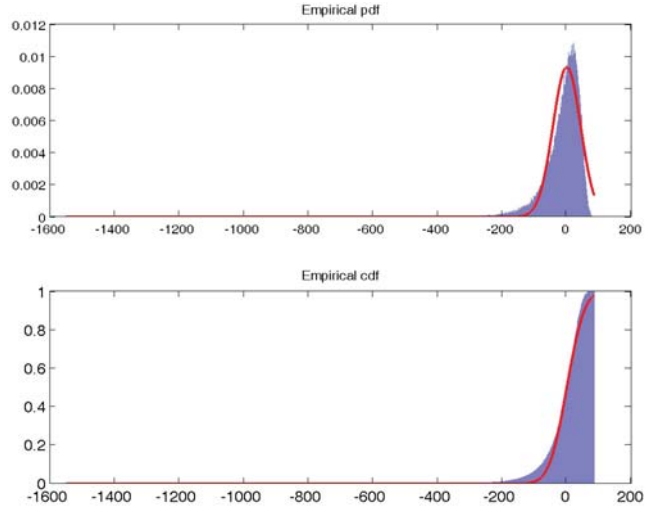


Fig. 5. Empirical pdf and cdf of \tilde{r}_i for Sensor 3 of Scenario 3.

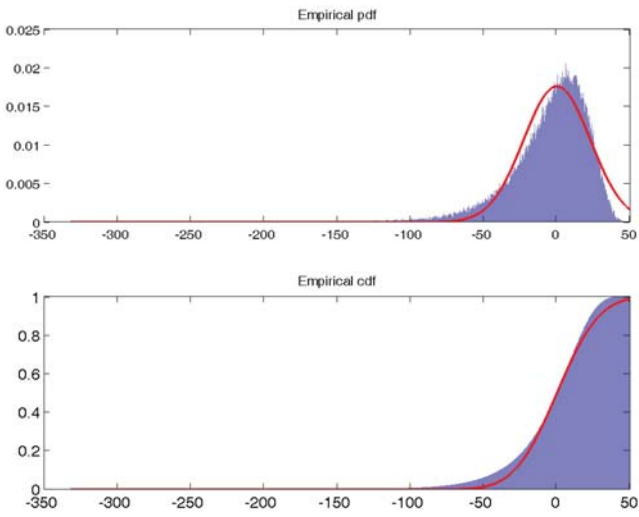


Fig. 4. Empirical pdf and cdf of \tilde{r}_i for Sensor 2 of Scenario 3.

negligible. For that reason, the simultaneous estimation of the sensor positions can reasonably be omitted from the overall estimation, but the effect of the sensor localization errors needs to be accounted for in the variances of ϕ_i and r_i , particularly when calculating the CRLB for use in determining the overall efficiency of the estimation scheme.

2.2. Range Estimate Error Distribution

The preceding section followed the analysis of [9], [10] with regards to the range estimation error

$$\tilde{r}_i = \hat{r}_i - r_i \quad (24)$$

where the range estimation error was assumed to be Gaussian distributed, i.e.,

$$\tilde{r}_i \sim \mathcal{N}(r_i, \sigma_{r_i}^2(T, S_i, \omega)) \quad (25)$$

where the variance is given by (10), or equivalently as

$$\sigma_{r_i}^2(T, S_i, \omega) = \frac{c^2 \sigma_r^2 + r_i^2 (\sigma_\phi^2 + \sigma_\varphi^2) \sin^2(\phi_i - \varphi_i)}{(1 - \cos(\phi_i - \varphi_i))^2} \quad (26)$$

In order to examine the Gaussian assumption on the range estimate errors, an empirical pdf and cdf (i.e., histograms) of the range estimate error was generated from 10^5 Monte Carlo simulations. The range estimates used to generate the empirical pdfs and cdfs were generated by (9) using the native measurements corrupted by Gaussian noise. The nonlinearity of (9) is what causes the range errors to be non-Gaussian.

The simulation parameters are set identically to Scenario 3 of Section 4. The empirical pdfs and cdfs are shown in Figures 3–5. Each figure, in addition to the histograms, is overlaid with the Gaussian pdf of (25). It is clear from these figures that the actual density of the range errors is not symmetric, and there is a heavier left tail than if the errors were indeed Gaussian.

2.3. Centralized Fusion

The estimates z_i and \hat{S}_i (or ζ_i and $\hat{\zeta}_i$) from each sensor are passed on to a fusion center in order to determine the estimate $\hat{\mathbf{x}}$ by means of the Iterated Least Squares (ILS) estimator⁴ [2]. The parameter vector to be estimated is

$$\mathbf{x} = [T_x \quad T_y \quad \omega \quad S_{1_x} \quad S_{1_y} \cdots S_{n_x} \quad S_{n_y}]' \quad (27)$$

with observations

$$\mathbf{y} = [\mathbf{y}'_1 \cdots \mathbf{y}'_n]' \quad (28)$$

where

$$\mathbf{y}_i = [z'_i \quad \hat{S}'_i]' \quad (29)$$

or with observations

$$\boldsymbol{\eta} = [\boldsymbol{\eta}'_1 \cdots \boldsymbol{\eta}'_n]' \quad (30)$$

where

$$\boldsymbol{\eta}_i = [\zeta'_i \quad \hat{\zeta}'_i]' \quad (31)$$

depending on whether the native measurements (31) or local estimates (29) are sent to the fusion center.

⁴Alternatively, Levenberg-Marquardt, or any other suitable nonlinear least squares solver may be used.

In order to use the ILS estimation algorithm, an initial estimate of \mathbf{x} is needed. It has been noted [9], [10] that the ILS estimator is sensitive to the initial estimate and may diverge if the initial estimate is too far from the truth.

While the initialization of the target position could be performed by using the bearing and range measurements (from the nodes with range measurements), the large variance of the range measurements was found to occasionally cause divergence in the ILS algorithm. A more robust initialization was found to follow a similar method to that used in [4]. This method of initialization utilizes only the available bearing measurements from each sensor (6), which can be rewritten as

$$\underbrace{\begin{bmatrix} \tan \phi_1 & -1 \\ \tan \phi_2 & -1 \\ \vdots & \vdots \\ \tan \phi_n & -1 \end{bmatrix}}_A T = \underbrace{\begin{bmatrix} S_{1_x} \tan \phi_1 - S_{1_y} \\ S_{2_x} \tan \phi_2 - S_{2_y} \\ \vdots \\ S_{n_x} \tan \phi_n - S_{n_y} \end{bmatrix}}_b \quad (32)$$

and T is obtained as

$$T = A^\dagger b \quad (33)$$

where A^\dagger is the (right) pseudo-inverse of A .

Also, note that (32) can be rewritten using the expression

$$\phi_i = \cot^{-1} \left(\frac{T_x - S_{i_x}}{T_y - S_{i_y}} \right) \quad (34)$$

which is simply (6) rewritten using the cotangent function. As suggested in [4], use of the cotangent function has been made when the measured bearing is between 45° and 135° or between -45° and -135° , in order to avoid the singularity of the tangent function around $\pm 90^\circ$.

To complete the initialization of \mathbf{x} , ω can be taken as the average of $\hat{\omega}_i$. If the native measurements are sent to the fusion center, the DOA shockwave estimates $\hat{\phi}_i$ can be used to solve for the equivalent $\hat{\omega}_i$ in order to initialize in the same manner.

Due to the nature of the DOA shockwave estimates (7) (which is one of two angles depending on which side of the bullet trajectory the sensor is located on), the predicted values of ϕ_i that must be calculated for the ILS algorithm may occasionally exhibit very large errors. This will occur if the errors on $\hat{\phi}_i$ and $\hat{\omega}_i$ are such that the i th sensor is predicted to appear on the incorrect side of the bullet trajectory. For this reason, when the native measurements are sent to the fusion center, the predicted value of ϕ_i will be given as whichever of the two possibilities is closest to the value of $\hat{\phi}_i$ sent to the fusion center. This is a reasonable solution to resolving the ambiguity since the errors of $\hat{\phi}_i$ will be assumed to be much smaller than the difference between the two values of ϕ_i .

3. CRAMER-RAO LOWER BOUND

The CRLB provides a lower bound on the covariance matrix of the estimate $\hat{\mathbf{x}}$ as

$$E[(\hat{\mathbf{x}} - \mathbf{x})(\hat{\mathbf{x}} - \mathbf{x})'] \geq J^{-1} \quad (35)$$

where J is the FIM

$$J = E\{[\nabla_{\mathbf{x}} \lambda(\mathbf{x})][\nabla_{\mathbf{x}} \lambda(\mathbf{x})]'\} \quad (36)$$

and $\lambda(\mathbf{x})$ is the negative log-likelihood function (NLLF).

3.1. Native Measurement Based FIM

The likelihood function of \mathbf{x} based on $\boldsymbol{\eta}$, assuming the sensor location estimate errors are independent of the native measurement errors, is

$$\Lambda_{\boldsymbol{\eta}}(\mathbf{x}) = \prod_{i=1}^n \Lambda_{\zeta_i}(T, S_i, \omega) \Lambda_{S_i}(S_i) \quad (37)$$

The NLLF corresponding to (37) is

$$\lambda_{\boldsymbol{\eta}}(\mathbf{x}) = \frac{1}{2} \sum_{i=1}^n (\boldsymbol{\eta}_i - \boldsymbol{\mu}_{\boldsymbol{\eta}_i}(\mathbf{x}))' \boldsymbol{\Sigma}_{\boldsymbol{\eta}_i}^{-1} (\boldsymbol{\eta}_i - \boldsymbol{\mu}_{\boldsymbol{\eta}_i}(\mathbf{x})) \quad (38)$$

where

$$\boldsymbol{\mu}_{\boldsymbol{\eta}_i} = [\mu'_{\zeta_i} \quad S'_i]' \quad (39)$$

$$\boldsymbol{\Sigma}_{\boldsymbol{\eta}_i} = \begin{bmatrix} \Sigma_{\zeta_i} & 0 \\ 0 & \Sigma_{S_i} \end{bmatrix} \quad (40)$$

and the unnecessary constant terms have been omitted. In this case, the FIM can be shown to be

$$J_{\boldsymbol{\eta}} = H'_{\boldsymbol{\eta}} \boldsymbol{\Sigma}_{\boldsymbol{\eta}}^{-1} H_{\boldsymbol{\eta}} \quad (41)$$

where

$$H_{\boldsymbol{\eta}} \triangleq \frac{\partial \boldsymbol{\mu}_{\boldsymbol{\eta}}(\mathbf{x})}{\partial \mathbf{x}} \quad (42)$$

is the Jacobian matrix of the native measurements,

$$\boldsymbol{\mu}_{\boldsymbol{\eta}}(\mathbf{x}) = [\mu_{\boldsymbol{\eta}_1}(\mathbf{x})', \dots, \mu_{\boldsymbol{\eta}_n}(\mathbf{x})']' \quad (43)$$

and

$$\boldsymbol{\Sigma}_{\boldsymbol{\eta}} = \begin{bmatrix} \Sigma_{\boldsymbol{\eta}_1} & 0 & 0 \\ 0 & \ddots & 0 \\ 0 & 0 & \Sigma_{\boldsymbol{\eta}_n} \end{bmatrix} \quad (44)$$

3.2. Local Estimate Based FIM

The likelihood function of \mathbf{x} based on \mathbf{y} follows similarly to (37). The corresponding NLLF is

$$\lambda_{\mathbf{y}}(\mathbf{x}) = \sum_{i=1}^n \left[\frac{1}{2} (\mathbf{y}_i - \boldsymbol{\mu}_{\mathbf{y}_i}(\mathbf{x}))' \boldsymbol{\Sigma}_{\mathbf{y}_i}(\mathbf{x})^{-1} (\mathbf{y}_i - \boldsymbol{\mu}_{\mathbf{y}_i}(\mathbf{x})) + \frac{1}{2} \ln |\boldsymbol{\Sigma}_{z_i}(\mathbf{x})| \right] \quad (45)$$

where

$$\boldsymbol{\mu}_{\mathbf{y}_i} = [\mu'_{z_i} \quad S'_i]' \quad (46)$$

$$\boldsymbol{\Sigma}_{\mathbf{y}_i}(\mathbf{x}) = \begin{bmatrix} \Sigma_{z_i}(\mathbf{x}) & 0 \\ 0 & \Sigma_{S_i} \end{bmatrix} \quad (47)$$

and the unnecessary constant terms have been omitted. Note that some entries of Σ_{z_i} are dependent on the target-sensor geometry. In this case, the FIM will be more complicated.

The FIM for the case of a multivariate Gaussian likelihood with parameter-dependent covariance is as follows [19]. The gradient terms of the FIM are

$$\begin{aligned} & \frac{\partial \lambda_{\mathbf{y}}(\mathbf{x})}{\partial x_j} \\ &= \frac{1}{2} \text{tr} \left(\Sigma_{\mathbf{y}}^{-1}(\mathbf{x}) \frac{\partial \Sigma_{\mathbf{y}}(\mathbf{x})}{\partial x_j} \right) \\ & \quad - \frac{1}{2} (\mathbf{y} - \mu_{\mathbf{y}}(\mathbf{x}))' \Sigma_{\mathbf{y}}^{-1}(\mathbf{x}) \frac{\partial \Sigma_{\mathbf{y}}(\mathbf{x})}{\partial x_j} \Sigma_{\mathbf{y}}^{-1}(\mathbf{x}) (\mathbf{y} - \mu_{\mathbf{y}}(\mathbf{x}))' \\ & \quad - \left[\frac{\partial \mu_{\mathbf{y}}(\mathbf{x})}{\partial x_j} \right]' \Sigma_{\mathbf{y}}^{-1}(\mathbf{x}) (\mathbf{y} - \mu_{\mathbf{y}}(\mathbf{x})) \end{aligned}$$

where x_j is the j th entry of \mathbf{x} . The (i, j) th entry in the FIM $J_{\mathbf{y}}$ is then

$$\begin{aligned} J_{i,j} &= \frac{1}{2} \text{tr} \left(\Sigma_{\mathbf{y}}^{-1}(\mathbf{x}) \frac{\partial \Sigma_{\mathbf{y}}(\mathbf{x})}{\partial x_j} \Sigma_{\mathbf{y}}^{-1}(\mathbf{x}) \frac{\partial \Sigma_{\mathbf{y}}(\mathbf{x})}{\partial x_i} \right) \\ & \quad + \left[\frac{\partial \mu_{\mathbf{y}}(\mathbf{x})}{\partial x_j} \right]' \Sigma_{\mathbf{y}}^{-1}(\mathbf{x}) \left[\frac{\partial \mu_{\mathbf{y}}(\mathbf{x})}{\partial x_i} \right] \end{aligned} \quad (48)$$

In order to compare bearings-only localization to the localization schemes presented here, the ‘‘bearings-only’’ FIM, J_b , must also be derived. It can be shown that J_b follows identically to (41), but with (42) and (44) modified to remove the portions dealing with φ_i and τ_i .

In all, three versions of the CRLB are evaluated in the sequel: the bearings-only CRLB, J_b^{-1} , the local estimate based CRLB, J_{η}^{-1} , and the native measurement CRLB, J_{η}^{-1} .

For the case of the local estimate based FIM J_{η} , appropriate care should be taken to adjust $\mu_{\mathbf{y}}(\mathbf{x})$ and $\Sigma_{\mathbf{y}}(\mathbf{x})$ for sensors that do not provide \hat{r}_i and $\hat{\omega}_i$. Additionally, in order to calculate the FIM from (48), the partial derivatives of $\sigma_{r_i}^2$, $\text{cov}(r_i, \phi_i)$, and $\text{cov}(r_i, \omega_i)$ are needed, as well as the partial derivatives of ϕ_i , r_i and ω . The expressions for the necessary partial derivatives can be found in Appendix B.

4. SIMULATION RESULTS

The simulation scenarios examined here include the scenarios of [9], [10] and an additional modified scenario with fewer sensors. For each scenario, the Mach number of the bullet is assumed to be $m = 2$, and the speed of sound is assumed to be $c = 342$ m/s. The measurement noise standard deviations are $\sigma_{\phi} = \sigma_{\varphi} = 4^\circ$, $\sigma_{\tau} = 1$ ms, and $\sigma_{i_x} = \sigma_{i_y} = 2$ m. The simulations were performed for 100 Monte Carlo runs for each scenario.

For each scenario, the fusion center estimates the vector \mathbf{x} of (27) via the ILS algorithm, using each of

the following sets of measurements:

- (i) the bearings-only case, with $\hat{\phi}_i$ and \hat{S}_i
- (ii) and the local estimate case, with z_i and \hat{S}_i
- (iii) the native measurement case, with ζ_i and \hat{S}_i

When the ILS algorithm is performed at the fusion center with the local estimates \hat{z}_i , the measurement noise covariance was modified from that of (16). Namely, the crosscovariance between ϕ_i and r_i , and the crosscovariance between ω_i and r_i are assumed to be zero. Even though these terms were found to be reasonably good approximations to the true crosscovariance between the range and angular errors, the ILS algorithm performed poorly when provided a measurement noise covariance containing these terms (results demonstrating this can be found in Figure 21).

In Scenarios 1 and 2, there are five sensor nodes located at (all positions are in m)

$$S = \begin{bmatrix} 127 & 20 & 90 & 136 & 182 \\ 107 & 22 & 0 & 68 & 59 \end{bmatrix} \quad (49)$$

In Scenario 1, the target is located at $T = [50, 50]'$ and the bullet is fired at a trajectory of $\omega = 30^\circ$ (counterclockwise from the x -axis). Due to the location of the sensors and the trajectory of the bullet, only sensors 1, 4 and 5 receive the shockwave and are able to send range and bullet trajectory estimates (or, equivalently, φ_i and τ_i in the native measurement case) to the fusion center.

The results of Scenario 1 are shown in Figures 6–8. Each figure shows the true locations of the target and sensors, along with the corresponding 95% error ellipses. Figure 6 shows the error ellipses corresponding to the sample covariance matrix (dashed line) calculated from the estimation errors over the 100 Monte Carlo runs when only bearing measurements are sent to the fusion center, and the covariance matrix from the bearings-only CRLB (solid line, denoted as CRLB_{bo}). Figure 7 shows the covariance matrix calculated from the estimation errors when the native measurements of ϕ , φ , and τ are available at the fusion center, and the covariance matrix from the native measurement CRLB (denoted as CRLB_{nm}). Figure 8 shows the covariance matrix calculated from the estimation errors when local estimates of range and bullet trajectory are available at the fusion center (in addition to bearing), and the covariance matrix from the local estimate based CRLB (denoted CRLB_{le}).

The covariance matrices from the CRLBs closely match the covariances of the estimation errors calculated from the simulation. This first indicates that the ILS estimation carried out by the fusion center is statistically efficient. Additionally, the fact that the bearings-only CRLB_{bo} and local estimate based CRLB_{le} matrices closely match suggests that very little information is gained from the range estimates sent from sensors 1, 4 and 5. The native measurement CRLB_{nm} matrix,

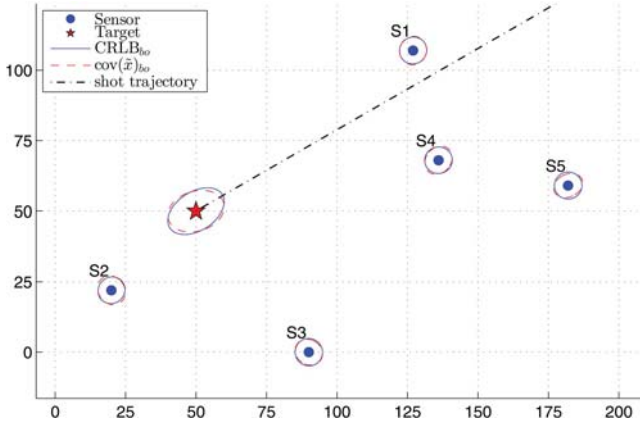


Fig. 6. Scenario 1, bearings-only $CRLB_{Bo}$ ellipses and error ellipses of estimated target and sensor locations (all 95%).

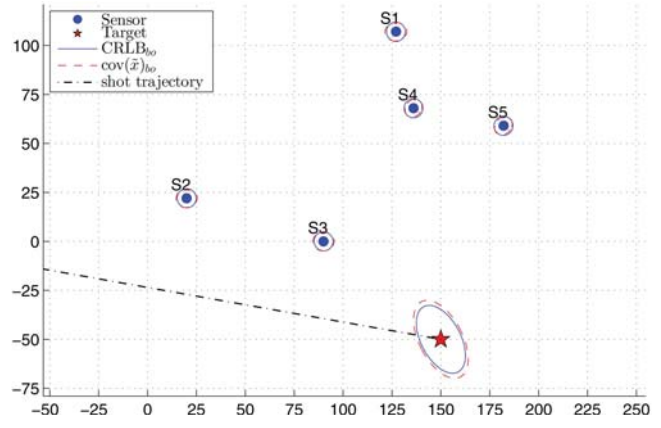


Fig. 9. Scenario 2, bearings-only $CRLB_{Bo}$ ellipses and error ellipses of estimated target and sensor locations (all 95%).

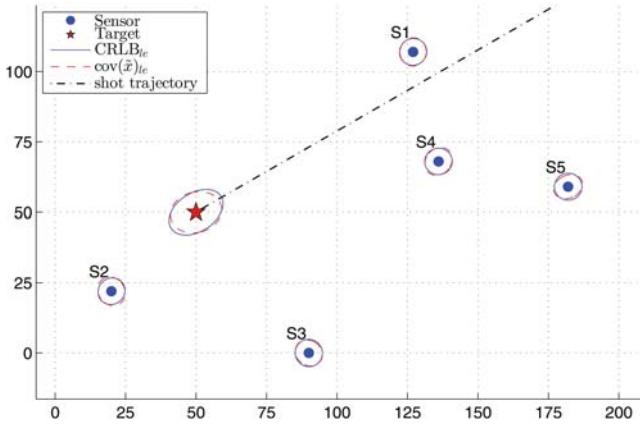


Fig. 7. Scenario 1, native measurement $CRLB_{nm}$ ellipses and error ellipses of estimated target and sensor locations (all 95%).

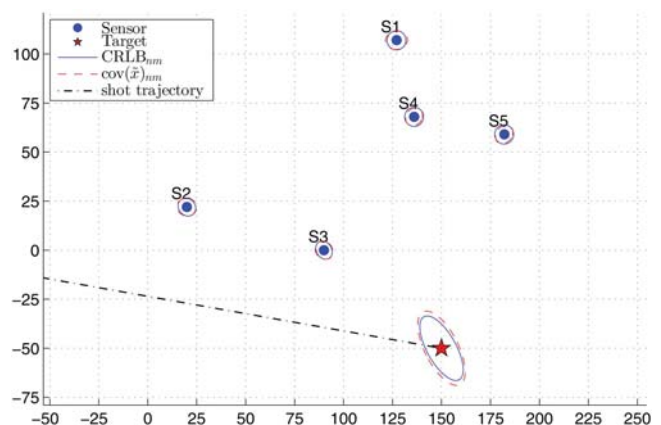


Fig. 10. Scenario 2, native measurement $CRLB_{nm}$ ellipses and error ellipses of estimated target and sensor locations (all 95%).

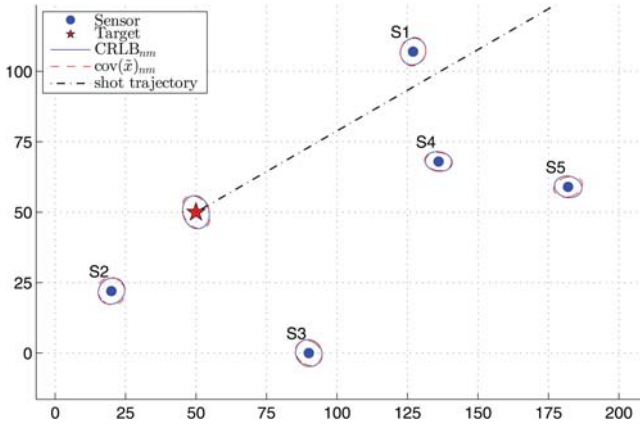


Fig. 8. Scenario 1, local estimate based $CRLB_{le}$ ellipses and error ellipses of estimated target and sensor locations (all 95%).

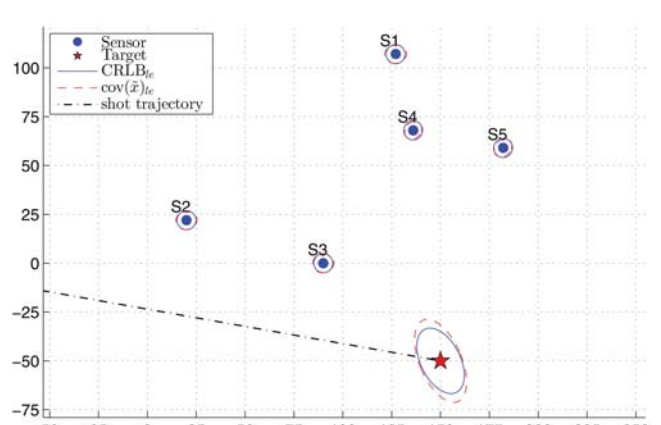


Fig. 11. Scenario 2, local estimate based $CRLB_{le}$ ellipses and error ellipses of estimated target and sensor locations (all 95%).

however, shows there is room for improvement of the target localization accuracy, which can be achieved by sending the native measurements to the fusion center.

In Scenario 2, the target is located at $T = [150, -50]'$ and the bullet is fired at a trajectory of $\omega = 170^\circ$. Due to the location of the sensors and the trajectory of the bullet, only sensors 2 and 3 receive the shockwave and are able to send range and bullet trajectory estimates to the fusion center.

The results of Scenario 2 are shown in Figures 9–11. Each figure once again shows the various 95% error ellipses. Figure 9 shows the error ellipses of the bearings-only $CRLB_{Bo}$ and the estimation errors, Figure 10 shows the error ellipses of the native measurement $CRLB_{nm}$ and estimation errors, and Figure 11 shows the error ellipses of the local estimate $CRLB_{le}$ and estimation errors.

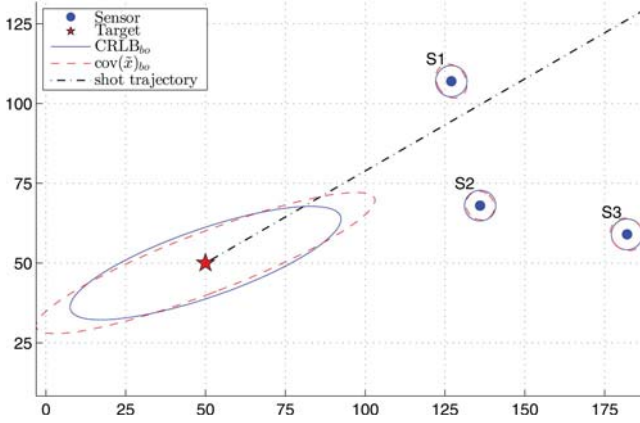


Fig. 12. Scenario 3, bearings-only CRLB_{Bo} ellipses and error ellipses of estimated target and sensor locations (all 95%).

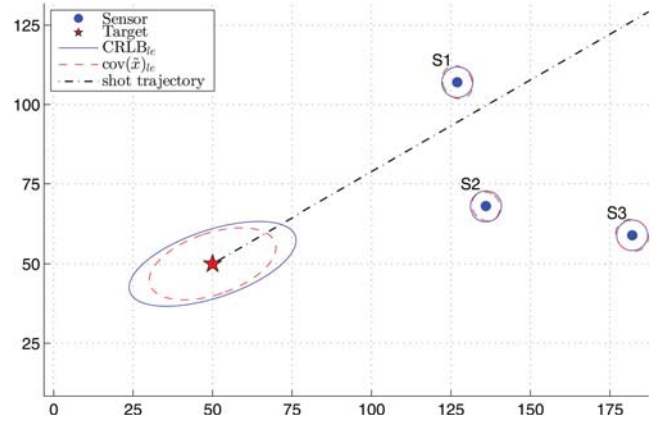


Fig. 14. Scenario 3, local estimate based CRLB_{Le} ellipses and error ellipses of estimated target and sensor locations (all 95%).

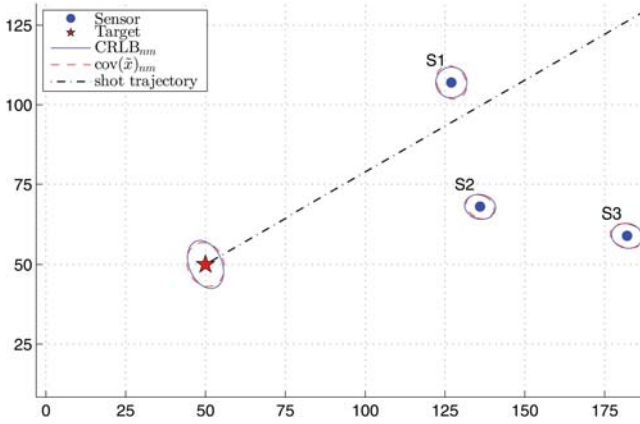


Fig. 13. Scenario 3, native measurement CRLB_{nm} ellipses and error ellipses of estimated target and sensor locations (all 95%).

The covariance matrices for all versions of the CRLB again closely match those obtained from the estimation errors, indicating that the estimator is once again efficient and the range estimates carry very little information. In this scenario, the advantage of sending the native measurements is minimal in comparison to Scenario 1.

Scenario 3 consists of an identical situation to Scenario 1, but with sensors 2 and 3 removed. In this case, the geometry of the sensors and target is poor, with each sensor having very similar line-of-sight (LOS) angles to the target.

The results of Scenario 3 are shown in Figures 12–14. In this case, the local estimate CRLB_{Le} and estimation errors are improved over the bearings-only case, and the native measurement case is considerably better than either of the alternatives. The covariance of the estimation errors of the bearings-only case does not match well to the corresponding CRLB, which suggests that the estimator may not be efficient in this case. A statistical hypothesis test for efficiency via the normalized estimation error squared (NEES) is carried out to more rigorously examine the statistical efficiency of each case.

The NEES for the source localization was examined for each scenario, using the bearings-only CRLB_{Bo} , the native measurement CRLB_{nm} , and the local estimate based CRLB_{Le} , to provide a statistical confirmation of the efficiency of the estimator. In each case, the CRLB was evaluated at the true \mathbf{x} . The NEES was calculated for the following:

- (i) the fused position estimation errors using bearings-only measurements with the bearings-only CRLB,
- (ii) the fused position estimation errors using local estimates with the local estimate based CRLB, and
- (iii) the fused position estimation errors using native measurements with the native measurement CRLB.

The NEES results (with the 95% probability region based on the chi-square distribution with two degrees of freedom and 100 Monte Carlo runs [2], being [1.63, 2.41]) are shown in Figures 15–17. Each scenario was simulated with multiple levels of angular measurement noise, namely, the standard deviations σ_ϕ and σ_φ were varied from 10% to 150% of their original value of 4° . The remaining measurement noise standard deviations remained the same as in the previous simulations.

The NEES results show that each estimation scheme is statistically efficient, with the exception of the bearings-only and local estimate based case of Scenario 3, and is “marginally” efficient for the local estimate based case of Scenario 2. The confidence region for the NEES assumes that the estimate errors are Gaussian distributed, which is an approximation in the local estimate case (see Section 2.2). For the more difficult geometry of Scenario 3, the bearings-only case loses efficiency for higher levels of angular measurement noise. Likewise, at very small levels of measurement noise, the local estimate scheme appears inefficient. This is likely due to the approximations involved in the range variance, and in the assumption that the range estimation errors are Gaussian distributed.

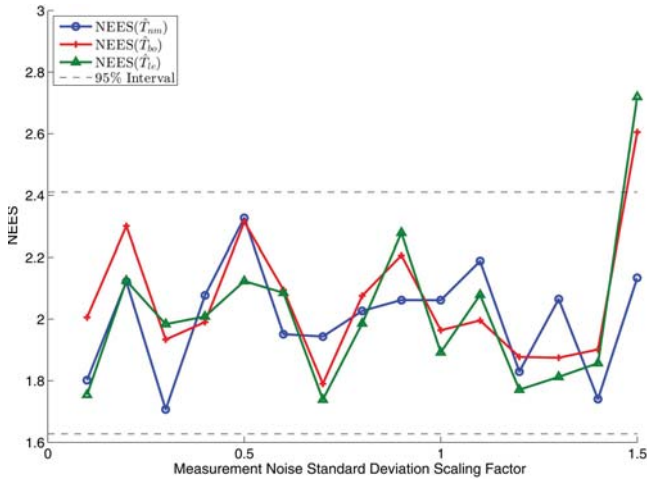


Fig. 15. Scenario 1, NEES for different levels of angular measurement noise.

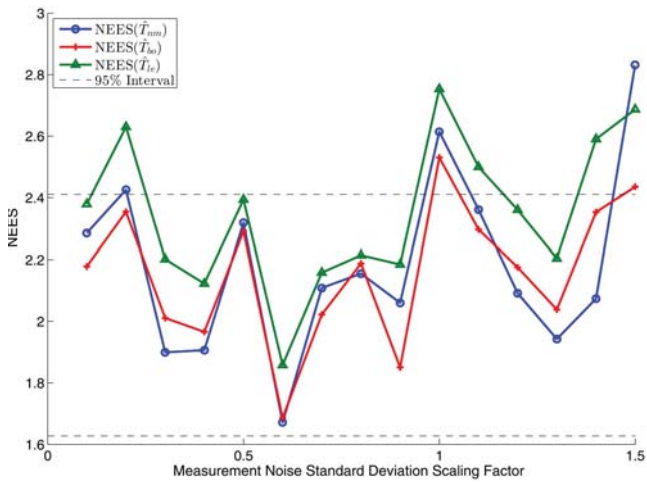


Fig. 16. Scenario 2, NEES for different levels of angular measurement noise.

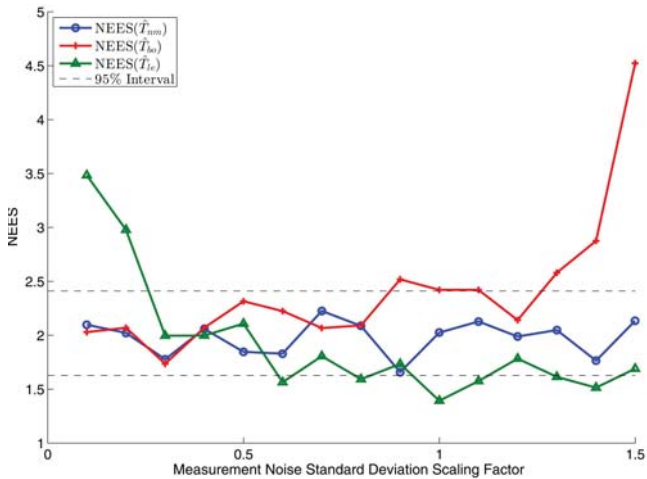


Fig. 17. Scenario 3, NEES for different levels of angular measurement noise.

Figures 18–20 show the target position root mean squared error (RMSE) (coordinate-combined) for Scenarios 1–3, along with the CRLB, for the bearings-only, native measurement, and local estimate cases.

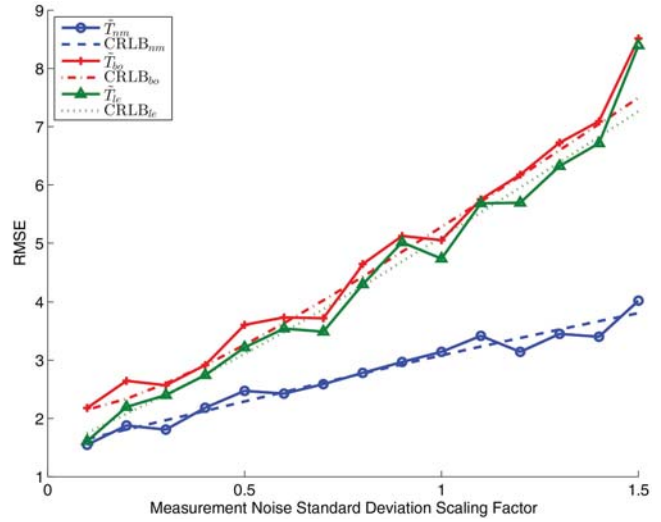


Fig. 18. Scenario 1, target position RMSE for different levels of angular measurement noise.

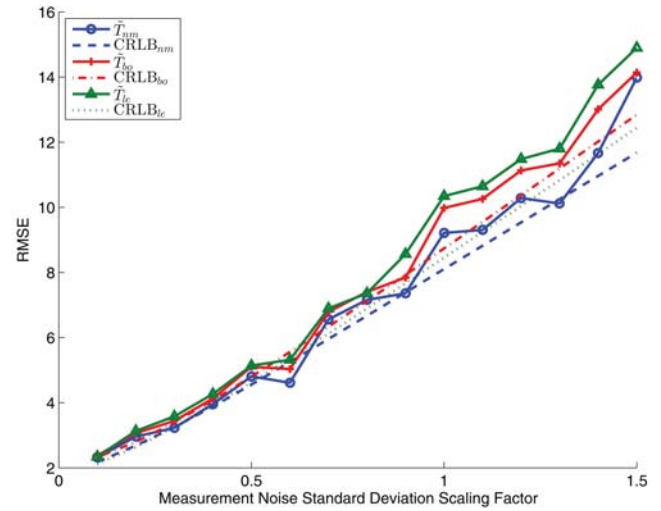


Fig. 19. Scenario 2, target position RMSE for different levels of angular measurement noise.

Figures 18 and 19 show that, over a range of angular measurement noise levels, the favorable geometry of Scenarios 1 and 2 provides for very little differentiation in the performance of target localization between the bearings-only and local estimate cases. Figure 20 shows that, for the less favorable geometry of Scenario 3, the inclusion of range estimates provides a significant increase in the accuracy of target localization. In both Scenarios 1 and 3, as seen in Figures 18 and 20, the native measurement case provides significantly improved target localization accuracy over the local estimate based case.

It should also be noted that Figure 20 appears to show the local estimate case outperforming its CRLB in Scenario 3. The CRLB in the local estimate case is necessarily approximate due to two factors in particular: namely, that the local estimates are assumed to have zero crosscovariances (because the use of approximate

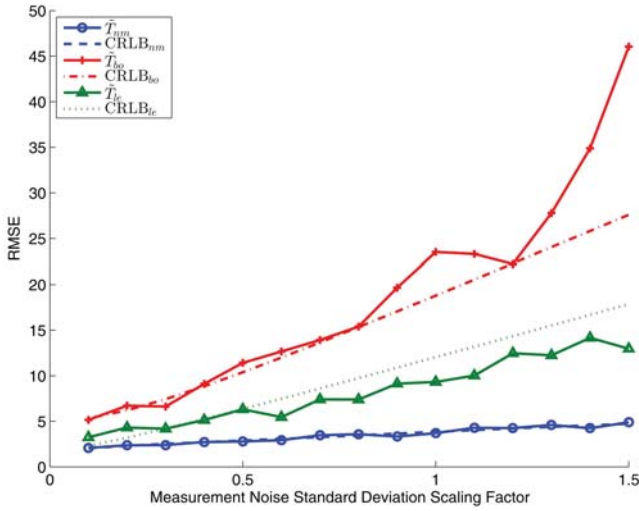


Fig. 20. Scenario 3, target position RMSE for different levels of angular measurement noise.

crosscovariances can cause instability in the search), even though the simulations result in non-zero cross-covariances; and the range errors are assumed Gaussian, which was demonstrated in Section 2.2 to be an approximation. Additionally, the affect of this approximation is not obvious when there is a more favorable geometry (e.g., Scenarios 1 and 2, where there are more (bearings-only) sensors present).

Note that in every case, $CRLB_{nm}$ is always lower than $CRLB_{le}$, and indeed the performance of the native measurements is always better than the local estimates. This is unsurprising as the local estimates are derived from the native measurements, and as such, cannot add any extra information beyond what exists in the native measurements. A better model for the distribution of the local estimates is likely needed to approach the performance of the native measurements.

Figure 21 shows an example run which demonstrates the reason for setting the crosscovariance terms of (16) to zero, rather than the (approximate) expressions provided in (17) and (18). Occasionally, when using these crosscovariance terms, the ILS search will diverge, whereas, this behavior is not observed when assuming there is no correlation between the local estimate errors. This divergence is caused by the cross-covariance terms causing (16) to become ill-conditioned, which causes difficulty in converging to the global maximum of the likelihood function (LF) surface. Note that in both cases, the local estimates are formed from the noisy native measurements, so there is indeed a correlation between the local estimate errors. The ILS algorithm must use the latest estimate to calculate the necessary terms of the covariance matrix, however, and it appears that the algorithm is more likely to diverge for non-zero crosscovariance terms. In fact, no divergence was observed in any run (in 3 scenarios, for 15 levels of

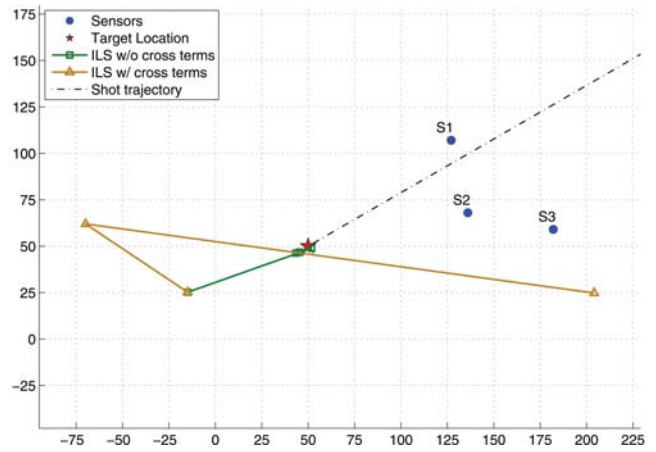


Fig. 21. Comparison of ILS iterations with and without approximate crosscovariance terms (the overlapping square and triangle represent the initial estimate).

measurement noise, with 100 runs each) when assuming zero crosscovariance.

Additionally, the different versions of the CRLB can be compared to gain insights into a particular scenario. The ratio of the area of the bearings-only $CRLB_{bo}$ ellipse to the local estimate based $CRLB_{le}$ ellipse can be calculated as $|(J_b^{-1})_T (J_y^{-1})_T^{-1}|^{1/2}$, where $(J^{-1})_T$ is the portion of the CRLB that deals with the target localization (as opposed to the entire vector \mathbf{x}). This is plotted over a two-dimensional (2-D) grid corresponding to various shooter locations in Figure 22, for sensor locations identical to Scenario 3. Each point in the 2-D grid corresponds to the ratio of the CRLB ellipse areas for a shooter at that location, shooting toward the marked aimpoint. Figure 22 clearly shows the shooter locations where the range measurements are most beneficial and the bearings-only localization will perform particularly poorly. Figure 23 shows the same results, only this time the native measurement $CRLB_{nm}$ is compared with the bearings-only $CRLB_{bo}$. Figure 23 shows a slightly different aimpoint in order to demonstrate the large difference in performance that is achieved when the bullet trajectory passes between different sensors. When the bullet trajectory passes on the same side of every sensor (which amounts to every sensor seeing the same shock-wave DOA φ) the performance is not much improved over either the bearings-only case or the local estimate based case (this is further demonstrated by the results of Scenario 2, which corresponds to such a sensor-target geometry). When the bullet trajectory passes between sensors (as in Scenario 1 and 3 above), the performance of the target localization is greatly improved by using the native measurements.

5. CONCLUSIONS

The CRLB and statistical efficiency were examined for multiple scenarios of a localization system using either native measurements or local estimates, where there are position-dependent noise terms. The system

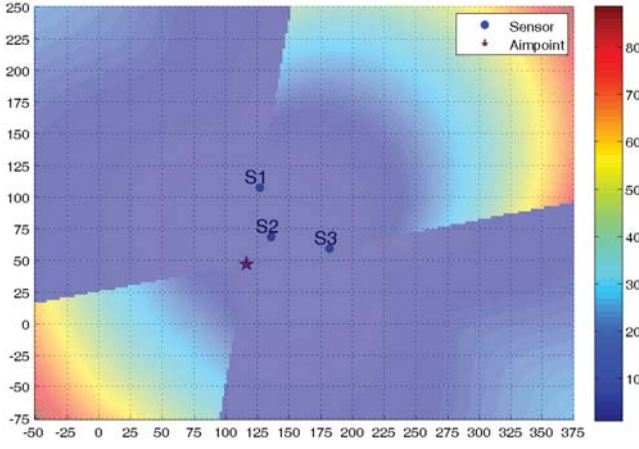


Fig. 22. Comparison of local estimate based $CRLB_{le}$ and bearings-only $CRLB_{bo}$ ($|(J_b^{-1})_T(J_y^{-1})_T^{-1}|^{1/2}$) over a 2-D grid (E-N, in m) of shooter position (for a fixed aimpoint at \star).

in question is a recently developed shooter localization scheme using acoustic gunfire detection sensors [9], [10]. The CRLB was derived for the cases of sensor nodes which send the following:

- (i) bearings only ($CRLB_{bo}$)
- (ii) bearing, range, and bullet trajectory estimates (“local estimate” based $CRLB_{le}$), and
- (iii) bearing, shockwave angle, and TDOA measurements (“native measurement” $CRLB_{nm}$)

When range estimates are passed to the fusion center in cases where the sensor-target geometry is favorable for angle-only localization, the bearings-only results (i) closely match the results of (ii), suggesting that there is little, if any, information contained in the range measurements in those cases. If the geometry is poor, however, as in Scenario 3, there is a significant difference between the bearings-only results (i) and the local estimate based results (ii). For each of the scenarios tested, when the native measurements are passed to the fusion center (iii), the localization accuracy was improved, with a significant improvement in Scenarios 1 and 3.

The distribution of the range estimate errors was also examined in order to highlight the approximation which is made when assuming the range errors to be Gaussian distributed. This assumption is likely the cause for the discrepancy in localization performance between the local estimate based case (ii) and the native measurement case (iii).

In each scenario, the NEES shows that the estimation is statistically efficient (with the exception of the bearings-only case with high measurement noise and a poor sensor-target geometry). When native measurements are passed to the fusion center, the localization is performed particularly well for the poor geometry of Scenario 3 and very closely matches the corresponding CRLB. The results show both that the estimator used in this particular acoustic localization system is efficient,

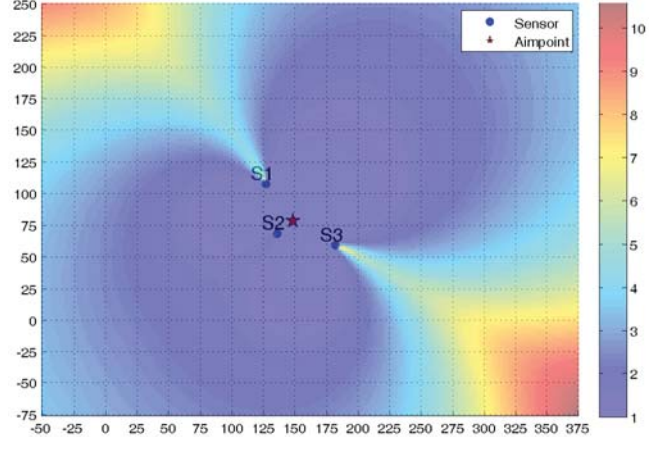


Fig. 23. Comparison of native measurement $CRLB_{nm}$ and bearings-only $CRLB_{bo}$ ($|(J_b^{-1})_T(J_\eta^{-1})_T^{-1}|^{1/2}$) over a 2-D grid (E-N, in m) of shooter position (for a fixed aimpoint at \star).

and that the CRLB can be used as an accurate means of performance prediction for such a system (particularly for the native measurement case).

APPENDIX A, COVARIANCE BETWEEN RANGE AND ANGULAR MEASUREMENTS

The i th sensor’s range measurement error \tilde{r}_i can be approximated (via Taylor series expansion) as

$$\tilde{r}_i \approx \frac{c\tilde{\tau}_i}{1 - \cos(\phi_i - \varphi_i)} - \frac{r_i \sin(\phi_i - \varphi_i)(\tilde{\phi}_i - \tilde{\varphi}_i)}{1 - \cos(\phi_i - \varphi_i)} \quad (50)$$

where $\tilde{\tau}_i$, $\tilde{\phi}_i$, and $\tilde{\varphi}_i$ are the errors of τ , ϕ_i , and φ_i , respectively.

In view of (50), the covariance between the i th sensor’s range and bearing measurement is

$$\begin{aligned} \text{cov}(r_i, \phi_i) &= E[\tilde{r}_i \tilde{\phi}_i] \\ &= -\frac{r_i \sin(\phi_i - \varphi_i)}{1 - \cos(\phi_i - \varphi_i)} \sigma_{\phi_i}^2 \end{aligned} \quad (51)$$

Similarly, the covariance between the i th sensor’s range and shockwave angle measurement is

$$\begin{aligned} \text{cov}(r_i, \omega) &= E[\tilde{r}_i \tilde{\varphi}_i] \\ &= \frac{r_i \sin(\phi_i - \varphi_i)}{1 - \cos(\phi_i - \varphi_i)} \sigma_{\varphi_i}^2 \end{aligned} \quad (52)$$

APPENDIX B, PARTIAL DERIVATIVE TERMS FOR LOCAL ESTIMATE FIM

In order to calculate the $\partial\mu(\mathbf{x})$ terms of (48), the partial derivatives of (6), (9) and ω are needed. The partial derivatives of (6) are

$$\frac{\partial\phi_i}{\partial T_x} = -\frac{T_y - S_{iy}}{r_i^2} \quad (53)$$

$$\frac{\partial\phi_i}{\partial T_y} = \frac{T_x - S_{ix}}{r_i^2} \quad (54)$$

$$\frac{\partial \phi_i}{\partial \omega} = 0 \quad (55)$$

$$\frac{\partial \phi_i}{\partial S_x} = \frac{T_y - S_{i_y}}{r_i^2} \quad (56)$$

$$\frac{\partial \phi_i}{\partial S_y} = -\frac{T_x - S_{i_x}}{r_i^2} \quad (57)$$

The partial derivatives of (9) are

$$\frac{\partial r_i}{\partial T_x} = \frac{T_x - S_{i_x}}{r_i} \quad (58)$$

$$\frac{\partial r_i}{\partial T_y} = \frac{T_y - S_{i_y}}{r_i} \quad (59)$$

$$\frac{\partial r_i}{\partial \omega} = 0 \quad (60)$$

$$\frac{\partial r_i}{\partial S_x} = -\frac{T_x - S_{i_x}}{r_i} \quad (61)$$

$$\frac{\partial r_i}{\partial S_y} = -\frac{T_y - S_{i_y}}{r_i} \quad (62)$$

The partial derivatives of ω are straightforward.

The $\partial \Sigma(\mathbf{x})$ terms of (48) require partial derivatives of (10), (17) and (18).

The partial derivatives of (10) are

$$\begin{aligned} \frac{\partial \sigma_r^2}{\partial \omega} &= \frac{2}{\sin(\phi_i - \varphi_i)} \left[\sigma_r^2 + \frac{c^2 \sigma_\tau^2 \cos(\phi_i - \varphi_i)}{(1 - \cos(\phi_i - \varphi_i))^2} \right] \\ &= \frac{2 \sin(\phi_i - \varphi_i)}{1 - \cos(\phi_i - \varphi_i)} \left[\sigma_r^2 - \frac{(\sigma_\phi^2 + \sigma_\varphi^2) r_i^2 \cos(\phi_i - \varphi_i)}{1 - \cos(\phi_i - \varphi_i)} \right] \end{aligned} \quad (63)$$

$$\begin{aligned} \frac{\partial \sigma_r^2}{\partial T_x} &= -\frac{\partial \phi_i}{\partial T_x} \frac{\partial \sigma_r^2}{\partial \omega} \\ &+ \frac{2(T_x - S_{i_x})(\sigma_\phi^2 + \sigma_\varphi^2) \sin^2(\phi_i - \varphi_i)}{(1 - \cos(\phi_i - \varphi_i))^2} \end{aligned} \quad (64)$$

$$\begin{aligned} \frac{\partial \sigma_r^2}{\partial T_y} &= -\frac{\partial \phi_i}{\partial T_y} \frac{\partial \sigma_r^2}{\partial \omega} \\ &+ \frac{2(T_y - S_{i_y})(\sigma_\phi^2 + \sigma_\varphi^2) \sin^2(\phi_i - \varphi_i)}{(1 - \cos(\phi_i - \varphi_i))^2} \end{aligned} \quad (65)$$

$$\frac{\partial \sigma_r^2}{\partial S_x} = -\frac{\partial \sigma_r^2}{\partial T_x} \quad (66)$$

$$\frac{\partial \sigma_r^2}{\partial S_y} = -\frac{\partial \sigma_r^2}{\partial T_y} \quad (67)$$

The partial derivatives of (17) are

$$\frac{\partial \text{cov}(r_i, \phi_i)}{\partial \omega} = -\frac{r_i \sigma_\phi^2}{1 - \cos(\phi_i - \varphi_i)} \quad (68)$$

$$\frac{\partial \text{cov}(r_i, \phi_i)}{\partial T_x} = -\frac{\partial \phi_i}{\partial T_x} \frac{\partial \text{cov}(r_i, \phi_i)}{\partial \omega} + \frac{\partial \phi_i}{\partial T_y} \text{cov}(r_i, \phi_i) \quad (69)$$

$$\frac{\partial \text{cov}(r_i, \phi_i)}{\partial T_y} = -\frac{\partial \phi_i}{\partial T_y} \frac{\partial \text{cov}(r_i, \phi_i)}{\partial \omega} - \frac{\partial \phi_i}{\partial T_x} \text{cov}(r_i, \phi_i) \quad (70)$$

$$\frac{\partial \text{cov}(r_i, \phi_i)}{\partial S_x} = -\frac{\partial \text{cov}(r_i, \phi_i)}{\partial T_x} \quad (71)$$

$$\frac{\partial \text{cov}(r_i, \phi_i)}{\partial S_y} = -\frac{\partial \text{cov}(r_i, \phi_i)}{\partial T_y} \quad (72)$$

The partial derivatives of (18) are

$$\frac{\partial \text{cov}(r_i, \omega_i)}{\partial \omega} = \frac{r_i \sigma_\varphi^2}{1 - \cos(\phi_i - \varphi_i)} \quad (73)$$

$$\frac{\partial \text{cov}(r_i, \omega_i)}{\partial T_x} = -\frac{\partial \phi_i}{\partial T_x} \frac{\partial \text{cov}(r_i, \omega_i)}{\partial \omega} + \frac{\partial \phi_i}{\partial T_y} \text{cov}(r_i, \omega_i) \quad (74)$$

$$\frac{\partial \text{cov}(r_i, \omega_i)}{\partial T_y} = -\frac{\partial \phi_i}{\partial T_y} \frac{\partial \text{cov}(r_i, \omega_i)}{\partial \omega} - \frac{\partial \phi_i}{\partial T_x} \text{cov}(r_i, \omega_i) \quad (75)$$

$$\frac{\partial \text{cov}(r_i, \omega_i)}{\partial S_x} = -\frac{\partial \text{cov}(r_i, \omega_i)}{\partial T_x} \quad (76)$$

$$\frac{\partial \text{cov}(r_i, \omega_i)}{\partial S_y} = -\frac{\partial \text{cov}(r_i, \omega_i)}{\partial T_y} \quad (77)$$

The $\partial \Sigma(\mathbf{x})$ terms of (48) can now be constructed from (63)–(77).

REFERENCES

- [1] J. Ash, G. Whipps, and R. Kozick "Performance of shockwave-based shooter localization under model misspecification," in *Acoustics Speech and Signal Processing (ICASSP), 2010 IEEE International Conference on*, 2010, pp. 2694–2697.
- [2] Y. Bar-Shalom, X.-R. Li, and T. Kirubarajan *Estimation with Applications to Tracking and Navigation: Theory, Algorithms and Software*. J. Wiley and Sons, 2001.
- [3] J. L. Crassidis, R. Alonso, and J. L. Junkins "Optimal Attitude and Position Determination from Line-of-Sight Measurements," *Journal of the Astronautical Sciences*, vol. 48(2), pp. 391–408, 2000.
- [4] D. F. Crouse, R. W. Osborne, III, K. Pattipati, P. Willett, and Y. Bar-Shalom "2D Location Estimation of Angle-Only Sensor Arrays Using Targets of Opportunity," in *13th International Conference on Information Fusion*, Edinburgh, UK, Jul. 2010, pp. 1–8.
- [5] T. Damarla, L. M. Kaplan, and G. T. Whipps "Sniper localization using acoustic asynchronous sensors," *IEEE Sensors Journal*, vol. 10, no. 9, pp. 1469–1478, Sep. 2010.
- [6] P. Fishbane, S. Gasiorowicz, and S. Thornton *Physics for Scientists and Engineers*, 2nd ed. Upper Saddle River, NJ: Prentice Hall, 1996, vol. 1, ch. 14, pp. 398–399.

- [7] W. H. Foy
“Position-Location Solutions by Taylor-Series Estimation,”
IEEE Trans. on Aerospace and Electronic Systems, vol. 12(2), pp. 187–194, Mar. 1976.
- [8] M. Gavish and A. J. Weiss
“Performance Analysis of Bearing-Only Target Location Algorithms,”
IEEE Trans. on Aerospace and Electronic Systems, vol. 28(3), pp. 817–828, Jul. 1992.
- [9] J. George and L. M. Kaplan
“Shooter Localization using Soldier-Worn Gunfire Detection Systems,”
in *14th International Conference on Information Fusion*, Chicago, IL, Jul. 2011, pp. 398–405.
- [10] J. George and L. M. Kaplan
“Shooter Localization using a Wireless Sensor Network of Soldier-Worn Gunfire Detection Systems,”
Journal of Advances in Information Fusion, vol. 8, no. 1, Jun. 2013.
- [11] D. Grasing and S. Desai
“Data fusion methods for small arms localization solutions,”
in *Information Fusion (FUSION), 2012 15th International Conference on*, 2012, pp. 713–718.
- [12] L. M. Kaplan, T. Damarla, and T. Pham
“QoI for Passive Acoustic Gunfire Localization,”
in *Mobile Ad Hoc and Sensor Systems, 2008. MASS 2008. 5th IEEE International Conference on*, Oct. 2008, pp. 754–759.
- [13] R. J. Kozick, J. George, L. M. Kaplan, and S. Deligeorges
“Centralized fusion of acoustic sensor data for gunfire localization,”
in *2011 MSS Battlespace Acoustic and Seismic Sensing, Magnetic and Electric Field Sensors (BAMS)*, Oct. 2011.
- [14] R. J. Kozick, G. T. Whipps, and J. N. Ash
“Supersonic projectile models for asynchronous shooter localization,”
in *Proc. SPIE Conf. Unattended Ground, Sea, and Air Sensor Technologies and Applications*, vol. 8046, May 2011.
- [15] P. Kuckertz, J. Ansari, J. Riihijarvi, and P. Mahonen
“Sniper fire localization using wireless sensor networks and genetic algorithm based data fusion,”
in *IEEE Military Communications Conference*, 2007, pp. 1–8.
- [16] D. Lindgren, O. Wilsson, F. Gustafsson, and H. Habberstad
“Shooter localization in wireless sensor networks,”
in *12th International Conference on Information Fusion*, Seattle, WA, 2009, pp. 404–411.
- [17] K. W. Lo and B. G. Ferguson
“Localization of small arms fire using acoustic measurements of muzzle blast and/or ballistic shock wave arrivals,”
J. Acoust. Soc. Am., vol. 132, no. 5, pp. 2997–3017, Nov. 2012.
- [18] R. W. Osborne, III and Y. Bar-Shalom
“Statistical Efficiency of Composite Position Measurements from Passive Sensors,”
in *Proc. SPIE Conf. Signal Processing, Sensor Fusion and Target Recognition*, vol. 8050-07, Orlando, FL, Apr. 2011.
- [19] B. Porat and B. Friedlander
“Computation of the Exact Information Matrix of Gaussian Time Series with Stationary Random Components,”
IEEE Trans. on Acoustics, Speech, and Signal Processing, vol. 34, no. 1, pp. 118–130, Feb. 1986.
- [20] J. Sallai, A. Lédeczi, and P. Völgyesi
“Acoustic shooter localization with a minimal number of single-channel wireless sensor nodes,”
in *Proceedings of the 9th ACM Conference on Embedded Networked Sensor Systems*, ser. SenSys ’11. New York, NY, USA: ACM, 2011, pp. 96–107. [Online]. Available: <http://doi.acm.org/10.1145/2070942.2070953>.
- [21] J. Sallai, P. Völgyesi, A. Lédeczi, K. Pence, T. Bapty, S. Neema, and J. R. Davis
“Acoustic shockwave-based bearing estimation,”
in *Proceedings of the 12th international conference on Information processing in sensor networks*, ser. IPSN ’13. New York, NY, USA: ACM, 2013, pp. 217–228. [Online]. Available: <http://doi.acm.org/10.1145/2461381.2461409>.
- [22] D. J. Torrieri
“Statistical Theory of Passive Location Systems,”
IEEE Trans. on Aerospace and Electronic Systems, vol. 20(2), pp. 183–198, Mar. 1984.
- [23] P. Volgyesi, G. Balogh, A. Nadas, C. B. Nash, and A. Ledeczi
“Shooter localization and weapon classification with soldier-wearable networked sensors,”
in *Proceedings of the 5th international conference on Mobile systems, applications and services*, ser. MobiSys ’07. New York, NY, USA: ACM, 2007, pp. 113–126. [Online]. Available: <http://doi.acm.org/10.1145/1247660.1247676>.
- [24] M. Wax
“Position Location from Sensors with Position Uncertainty,”
IEEE Trans. on Aerospace and Electronic Systems, vol. 19(5), pp. 658–662, Sep. 1983.
- [25] Y. Zhao, D. Yi, Y. Li, and Q. Zhang
“CRLB of Initial State Estimation for Boost Phase Object Based on 8-State Gravity Turn Model Using Space-Based Observations,”
in *2010 2nd International Conference on Signal Processing Systems (ICSPS)*, vol. 1, Dalian, China, Jul. 2010, pp. 781–789.



Richard W. Osborne, III obtained his B.S., M.S., and Ph.D. degrees in electrical engineering from the University of Connecticut in 2004, 2007, and 2012, respectively. He is currently an Assistant Research Professor in the Electrical Engineering department at the University of Connecticut, Storrs, CT. His academic interests include adaptive target tracking, information/sensor fusion, machine vision, and other aspects of estimation.

Yaakov Bar-Shalom was born on May 11, 1941. He received the B.S. and M.S. degrees from the Technion, Israel Institute of Technology, in 1963 and 1967 and the Ph.D. degree from Princeton University in 1970, all in electrical engineering. From 1970 to 1976 he was with Systems Control, Inc., Palo Alto, California. Currently he is Board of Trustees Distinguished Professor in the Dept. of Electrical and Computer Engineering and Marianne E. Klewin Professor in Engineering at the University of Connecticut. He is also Director of the ESP (Estimation and Signal Processing) Lab. His current research interests are in estimation theory, target tracking and data fusion. He has published over 500 papers and book chapters in these areas and in stochastic adaptive control. He coauthored the monograph *Tracking and Data Association* (Academic Press, 1988), the graduate texts *Estimation and Tracking: Principles, Techniques and Software* (Artech House, 1993), *Estimation with Applications to Tracking and Navigation: Algorithms and Software for Information Extraction* (Wiley, 2001), the advanced graduate texts *Multitarget-Multisensor Tracking: Principles and Techniques* (YBS Publishing, 1995), *Tracking and Data Fusion* (YBS Publishing, 2011), and edited the books *Multitarget-Multisensor Tracking: Applications and Advances* (Artech House, Vol. I, 1990; Vol. II, 1992; Vol. III, 2000). He has been elected Fellow of IEEE for “contributions to the theory of stochastic systems and of multi-target tracking.” He has been consulting to numerous companies and government agencies, and originated the series of Multitarget-Multisensor Tracking short courses offered via UCLA Extension, at Government Laboratories, private companies and overseas. During 1976 and 1977 he served as Associate Editor of the IEEE Transactions on Automatic Control and from 1978 to 1981 as Associate Editor of Automatica. He was Program Chairman of the 1982 American Control Conference, General Chairman of the 1985 ACC, and Co-Chairman of the 1989 IEEE International Conference on Control and Applications. During 1983–87 he served as Chairman of the Conference Activities Board of the IEEE Control Systems Society and during 1987–89 was a member of the Board of Governors of the IEEE CSS. He was a member of the Board of Directors of the International Society of Information Fusion (1999–2004) and served as General Chairman of FUSION 2000, President of ISIF in 2000 and 2002 and Vice President for Publications in 2004–13. In 1987 he received the IEEE CSS Distinguished Member Award. Since 1995 he is a Distinguished Lecturer of the IEEE AESS and has given numerous keynote addresses at major national and international conferences. He is co-recipient of the M. Barry Carlton Award for the best paper in the IEEE Transactions on Aerospace and Electronic Systems in 1995 and 2000 and recipient of the 1998 University of Connecticut AAUP Excellence Award for Research. In 2002 he received the J. Mignona Data Fusion Award from the DoD JDL Data Fusion Group. He is a member of the Connecticut Academy of Science and Engineering. In 2008 he was awarded the IEEE Dennis J. Picard Medal for Radar Technologies and Applications, and in 2012 the Connecticut Medal of Technology. He has been listed by academic.research.microsoft.com (top authors in engineering) as #1 among the researchers in Aerospace Engineering based on the citations of his work.





Jemin George received his M.S. ('07), and Ph.D. ('10) in Aerospace Engineering from the State University of New York at Buffalo. In 2008, he was a Summer Research Scholar with the U.S. Air Force Research Laboratory's Space Vehicles Directorate at Kirtland Air Force Base in Albuquerque, New Mexico. He was a National Aeronautics and Space Administration Langley Aerospace Research Summer Scholar with the Langley Research Center in 2009. From 2009–2010 he was a Research Fellow with the Stochastic Research Group, Department of Mathematics, Technische Universitat Darmstadt, Darmstadt, Germany. He joined ARL in 2010 as a civilian employee and is currently with the Networked Sensing & Fusion Branch of the Signal & Image Processing Division. He has published over 30 refereed technical articles in the areas of estimation, control and information fusion. He received the 2012 Army Research and Development Achievement Award for Outstanding Collaboration. He has chaired numerous technical conference sessions at the Institute of Electrical and Electronics Engineers (IEEE) American Control Conference (ACC), Society for Industrial and Applied Mathematics (SIAM) Conference on Uncertainty Quantification, and The American Institute of Aeronautics and Astronautics (AIAA) Guidance, Navigation and Control Conference. He currently serves on the Technical Program Committee for the International Conference on Information Fusion (FUSION) and as the Associate Editor for Contributed Papers for the ACC. His principal research interests include stochastic systems, control theory, nonlinear filtering, information fusion, adaptive networks, distributed sensing and estimation.



Lance Kaplan received the B.S. degree with distinction from Duke University, Durham, NC, in 1989 and the M.S. and Ph.D. degrees from the University of Southern California, Los Angeles, in 1991 and 1994, respectively, all in Electrical Engineering. From 1987–1990, Dr. Kaplan worked as a Technical Assistant at the Georgia Tech Research Institute. He held a National Science Foundation Graduate Fellowship and a USC Dean's Merit Fellowship from 1990–1993, and worked as a Research Assistant in the Signal and Image Processing Institute at the University of Southern California from 1993–1994. Then, he worked on staff in the Reconnaissance Systems Department of the Hughes Aircraft Company from 1994–1996. From 1996–2004, he was a member of the faculty in the Department of Engineering and a senior investigator in the Center of Theoretical Studies of Physical Systems (CTSPS) at Clark Atlanta University (CAU), Atlanta, GA. Currently, he is a researcher in the Networked Sensing and Fusion branch of the U.S. Army Research Laboratory. Dr. Kaplan serves as Editor-In-Chief for the IEEE Transactions on Aerospace and Electronic Systems (AES). In addition, he also serves on the Board of Governors of the IEEE AES Society and on the Board of Directors of the International Society of Information Fusion. He is a three time recipient of the Clark Atlanta University Electrical Engineering Instructional Excellence Award from 1999–2001. His current research interests include signal and image processing, automatic target recognition, information/data fusion, and resource management.